Article

Not peer-reviewed version

Modifications of phase morphology, physical properties and burning anti-dripping performance of compatibilized poly(butylene succinate)/high density polyethylene blend by adding nanofillers

Kartik Behera , Chien-Hsing Tsai , Yen-Hsiang Chang , Fang-Chyou Chiu *

Posted Date: 18 October 2023

doi: 10.20944/preprints202310.1171.v1

Keywords: poly(butylene succinate); high density polyethylene; blend; nanofillers; anti-dripping; physical properties.

Article

Modifications of Phase Morphology, Physical Properties and Burning Anti-Dripping Performance of Compatibilized Poly(Butylene Succinate)/High Density Polyethylene Blend by Adding Nanofillers

Kartik Behera [1], Chien-Hsing Tsai [1], Yen-Hsiang Chang [2] and Fang-Chyou Chiu [1,2]*

[1] Department of Chemical and Materials Engineering, Chang Gung University, Taoyuan 333, Taiwan ROC b.kartik1991@gmail.com (K.B.); a0970600013@gmail.com (C.-H.T.)
[2] Department of General Dentistry, Chang Gung Memorial Hospital, Taoyuan 333, Taiwan ROC cyh4714@hotmail.com (Y.-H.C.)
* Correspondence: maxson@mail.cgu.edu.tw(F.-C.C.) .

Abstract: A twin-screw extruder was used to fabricate poly(butylene succinate) (PBS)/high density polyethylene (HDPE) blends (7:3 weight ratio) and blend-based nanocomposites. Carbon nanotubes (CNTs), graphene nanoplatelets (GNPs) and organoclays (15A and 30B) served as the nanofiller, while maleated HDPE (PEgMA) acted as an efficient compatibilizer for the blend. In the composites, individual nanofillers were mostly localized in HDPE domains, but some fillers were also observed at PBS-HDPE interfaces. The sea-island morphology of compatibilized blend evolved into a pseudo-co-continuous morphology in the composites. Differential scanning calorimetry results confirmed that PEgMA with HDPE evidently accelerated the crystallization of PBS in the blend. The possible nucleation effect of added fillers on PBS crystallization was obscured by the formation of quasi-connected HDPE domains, causing less PBS nucleation sites. The presence of nanofillers improved the thermal stability and burning anti-dripping behavior of the parent blend. The anti-dripping efficiency of added fillers followed the sequence: CNT>15A>30B>GNP. Rigidity of the blend was increased after formation of nanocomposites. In particular, adding GNP resulted in 31% increase in flexural modulus. Development of a pseudo-network structure in the composites was confirmed by measurement of rheological properties. Electrical resistivity of the blend was reduced by more than 6 orders of magnitude at 3 phr CNT loading, demonstrating the achievement of double percolation morphology.

Keywords: poly(butylene succinate); high density polyethylene; blend; nanofillers; anti-dripping; physical properties

1. Introduction

Polymeric products have gained widespread use in daily life. However, the majority of them are made with a single-component polymer, which may not possess the necessary properties to fully meet the demands of individuals. Therefore, the development of polymeric materials is oriented towards multi-component blends and composites consisting of different polymers and fillers, which have better properties than the individual polymers [1,2]. For instance, the modification of electrical properties can be accomplished by loading conductive fillers into the polymer matrix to form composites [3–5]. Nanocomposite-based technology has enhanced the physical properties of various polymers and polymer blends by incorporating suitable nanofillers. In order to achieve high performance polymer nanocomposites, the polymer matrix and nanofiller must be compatible, and the nanofiller must be effectively dispersed in the matrix. Of the nanofillers, carbon nanotubes (CNTs), graphene nanoplatelets (GNPs) and organoclays are intensively investigated because of

 doi:10.20944/preprints202310.1171.v1

their exceptional aspect ratio and unique properties for improving properties of polymer matrices [6–8].

Poly(butylene succinate) (PBS) is synthesized from the monomers of succinic acid and 1,4-butanediol. Its fine mechanical/thermal properties and processability make PBS one of the most promising sustainable (biodegradable) aliphatic polyesters [9–11]. PBS is widely used in textiles, monofilaments, packaging and medical products [12–14]. However, its relatively high cost, low melt viscosity, limited gas barrier properties and inadequate toughness hinder its commercial feasibility in further applications [15,16]. These shortcomings are expected to be overcome by fabricating PBS-based blends and (nano)composites. The impact of the polarity of two types of organoclay (I.28E and I.34TCN) on the crystallization behavior of PBS was studied and compared by Teng et al. [17]. The crystallization of PBS was significantly improved during isothermal crystallization in the presence of organoclay, with stronger polarity clay exhibiting a greater effect than clay with weaker polarity. Yuan et al. [18] fabricated PBS/CNT nanocomposites and studied their crystallization kinetics and rheological properties. Good dispersion of CNTs was achieved at low content, while high CNT content resulted in poor dispersion and agglomeration. CNTs significantly enhanced the crystallization of PBS, resulting in a faster overall crystallization rate. Composites showed elastic characteristics due to the pseudo-network structure formation of CNTs. Platnieks et al. [19] investigated the physical properties of PBS/GNP composites. The crystallinity of PBS increased at 0.5 and 1.0% GNP loadings, whereas crystallinity decreased with higher GNP loadings. Thermal conductivity of PBS increased with increasing GNP loading.

Polyethylene (PE) is a widely used commodity polymer, known for its good mechanical/thermal properties, processability and low cost. The applications of PE were further broadened by blending with other polymers and/or loading with various fillers [20–22]. However, the widespread utilization of non-sustainable PE has resulted in severe, long-lasting environmental and waste management issues [23]. A realistic solution to mitigate the harmful effects is to produce PE blends with biopolymers such as PBS. PBS/PE blend shows an immiscible characteristic and has poor physical properties due to a lack of interaction between PBS and PE. Studies have focused on using PE grafted with maleic anhydride (PEgMA) as a compatibilizer/coupling agent to increase the interfacial interaction between PE and its blend counterparts or added fillers.

Minkova et al. [24] conducted an investigation on the thermal properties and microhardness of high density polyethylene (HDPE)/15A nanocomposites. PEgMA, ethylene–acrylic acid copolymer (EAA) and acrylic acid grafted PE (PEAA) acted individually as compatibilizers for composite preparation. Composites that contained PEAA and PEgMA had higher microhardness, thermal stability and flame-retardant properties than composites with EAA incorporated. Aontee et al. [25] studied the influence of PEgMA on the mechanical/thermal characteristics and crystallinity of PBS/HDPE-30/70 blend. The presence of 8 phr PEgMA significantly decreased the crystallinity of the PBS and HDPE. The addition of 2 phr PEgMA increased the tensile strength and elongation at break of the parent PBS/HDPE blend. Kodjie et al. [26] fabricated HDPE/CNT composites by a solvent casting method. Thermal stability of composites drastically improved due to the radical scavenging function of the added CNTs. The heterogeneous nucleation effect of CNTs was found to result in increased crystallization temperature of HDPE. Tarani et al. [27] investigated the effect of GNPs with different diameters of 5, 15 and 25 μm on the crystallization kinetics of HDPE. The inclusion of GNPs to HDPE led to a rise in the crystallization temperature. Specifically, the use of GNP M5 (5 μm), which had a smaller diameter, was found to increase the number of heterogeneous nucleation sites, leading to an acceleration in the crystallization rate. Moraweic et al. [28] fabricated nanocomposites by melt blending of low density polyethylene (LDPE) and organoclay. The compatibility of LDPE-organoclay was improved through the addition of PEgMA as a coupling agent. Transmission electron microscopy (TEM) analysis results revealed that the organoclay in the nanocomposite was dispersed in an exfoliated state. The crystallization temperature of LDPE in composites remained unaltered, as the clay lacked nucleation capability for LDPE. The composites showed better thermal stability than neat LDPE.

Nanocomposite systems made from multi-component polymer blends have been successfully fabricated and characterized for their potential in cutting-edge applications [3,29–31]. There have been studies exploring the versatility of PBS and HDPE blend-based composites. Darshan et al. [5] fabricated PBS/HDPE/CNT nanocomposites, using PEgMA as a compatibilizer. PEgMA enhanced the compatibility between the two components, while incorporating CNTs increased the thermal stability of the HDPE component. Young's modulus (YM) of the composite with 3-phr CNT inclusion showed a 50% increase compared with neat PBS. Wu et al. [32] fabricated PBS/PLA/nitrogen-doped graphene (NG) composites, and studied their morphology and physical properties. NG was mostly dispersed in the PBS-matrix, although little amount of NG was observed in PLA domains. NG improved miscibility in PBS/PLA-70/30 blend, resulting in smaller and finely dispersed PLA domains. The inclusion of NG also improved the thermal stability of PBS/PLA blend. NG loading of 1 wt.% significantly improved the PBS/PLA blend's tensile properties and dynamic storage/loss moduli. Polypropylene grafted with maleic anhydride (PPgMA) and CNT/organoclay (15A) were used as compatibilizer and nanofillers, respectively, for the successful fabrication of PBS/PP blend-based nanocomposites. CNTs were dispersed in both PP and PBS phases, while 15A was selectively localized in the PBS phase, leading to formation of a pseudo-co-continuous PP-PBS morphology. Composites with 2.5-phr CNT loading revealed significantly improved YM of the parent blend [8]. HDPE/PP/maleated rubber (EPDM-MA)/15A nanocomposites were fabricated by the melt blending method. The loading of 15A enhanced the PP crystallization, while the crystallization of HDPE was barely affected. The composites revealed improved thermal stability compared with the parent blend. Composites with 15A loading showed significantly increased tensile and flexural properties [33].

In the literature, only a few studies were conducted on blend-based nanocomposites loaded with different nanofillers. The comparison of adding various individual nanofillers on the modification of phase morphology and physical properties of immiscible polymer blends merits comprehensive investigation in order to broaden the blends' applications. The present study evaluated the impact of individual incorporation of CNTs, GNPs and organoclays on the physical characteristics of PEgMA compatibilized PBS/HDPE blend [5]. The phase morphology and dispersion of nanofillers in the composites, and the thermal properties, burning anti-dripping performance, mechanical properties, electrical resistivity and rheological behavior of the resultant blends and nanocomposites were determined and compared. The loading with CNTs showed potential for application of the composites in the anti-static and electromagnetic interference fields.

2. Materials and Methods

2.1. Materials and Sample Preparation

PBS (Bionolle #1001) with a weight average molecular weight (M_W) of 13.2×104 g/mol was purchased from Showa Denko K.K. (Japan), and HDPE (Taisox 8050) with M_W of 2.8×104 g/mol was obtained from Formosa Plastic Corporation, Taiwan. Maleic anhydride-grafted HDPE (coded as PEgMA, Fusabond MB100D), purchased from DuPont Co, was used as a compatibilizer for the blend. Organically modified montmorillonites, named Cloisite® 15A and Cloisite® 30B (coded as 15A and 30B, respectively), were purchased from Southern Clay Products, USA. The organic modifiers used for 15A and 30B were detailed in previous reports [3]. 15A possesses lower polarity compared with 30B. Multi-walled CNTs (grade ICT-030), having a diameter of 40–90 nm and carbon purity of >90%, were obtained from Golden Innovation Business Co. Ltd., Taiwan. GNPs (grade M-5) with an average lateral dimension of 5 μm were obtained from XG-Sciences, USA.

PBS, HDPE, PEgMA and nanofillers were first dried in a vacuum oven at 70°C for 24 h. A co-rotating twin-screw extruder (SHJ-20B, L/D = 40) was used to fabricate all the samples tested, including the neat blend components. The mixing temperature from hopper to die was 170 to 190°C, and the screw speed was 360 rpm. The extruded and pelletized samples were then molded into various ASTM standard specimens using an injection molding machine (V4-20SP-G, Multiplas

 doi:10.20944/preprints202310.1171.v1

Enterprise Co., Ltd., Taiwan) for further characterization. Table 1 recorded the designations of the samples.

Table 1. Samples designation and formulation.

Sample code	Composition	Parts (wt%)
PBS	PBS	100
HDPE	HDPE	100
S7E3	PBS/HDPE	70/30
S7E3M	PBS/HDPE/PEgMA	70/25/5
S7E3MA3	PBS/HDPE/PEgMA/15A	70/25/5/3*
S7E3MB3	PBS/HDPE/PEgMA/30B	70/25/5/3*
S7E3MT3	PBS/HDPE/PEgMA/CNT	70/25/5/3*
S7E3MG3	PBS/HDPE/PEgMA/GNP	70/25/5/3*

*: parts per hundred polymer resins (phr).

2.2. Characterization

Phase morphology of the blends/composites was observed using scanning electron microscopes (Hitachi S-3000N SEM and Jeol JSM-7500F FESEM). Prior to observations, the samples underwent cryogenic fracturing in liquid N_2 and sputter coated with gold. Transmission electron microscopy (TEM) was used to assess nanofiller dispersion in the blend matrix using a Jeol JEM-2000EX II at 100 kV. Ultrathin sections of the specimens of about 100 nm were prepared by a cryomicrotome (LEICA ULTRACUTR) fortified with a diamond knife at -130°C. The crystallization and melting behavior of the samples was investigated using differential scanning calorimetry (DSC Q10, TA Instruments) under a nitrogen environment. After melting at 200°C for 3 min, the crystallization behavior of the samples was recorded on cooling at a rate of 10°C/min. Subsequently, the samples were heated to 200°C at 20°C/min to assess the melting behavior. Samples were tested for thermal stability using a TGA TA Q50 thermogravimetric analyzer at a heating rate of 10°C/min from room temperature to 700°C under nitrogen environment.

An X-ray diffractometer with a monochromatic CuKα (λ = 1.54 Å) source was used for crystal structure assessment. Behera et al. [3,6] described a burning test to evaluate the anti-dripping behavior of fabricated specimens. Specimens (63.0 × 12.5 × 3.0 mm^3) were brought into direct contact with the flame of an alcohol lamp for 10 s, and then removed from the flame to observe subsequent burning/dripping behavior.

Tensile and flexural moduli of specimens in accordance with ASTM D638 and ASTM D790, respectively, were determined using a Gotech testing machine (AI-3000, Taiwan). Experiments were carried out with a crosshead speed of 10 mm/min or 1 mm/min at room temperature for tensile and flexural tests, respectively. The reported value for each formulation is an average of at least six independent tests. The rheological properties were studied using an Anton-Paar Physica rheometer (MCR 101) at 170°C in parallel plate geometry (25 mm in diameter, 10 mm in thickness) at 1% strain amplitude. The selected samples were measured for electrical resistivity using Mitsubishi Chemical Co. MCP-HT450 and MCP-T700 resistivity meters at room temperature.

3. Results and Discussion

3.1. Phase morphology and selective localization of nanofiller(s)

Figure 1 depicts the SEM images of the blends and composites. As shown in Figure 1(a), the S7E3 blend displayed phase-separated (sea-island) morphology, demonstrating its immiscible characteristic. The size of the dispersed HDPE domains (30 wt.% and 36 vol.%), ranged from 2 to 7 μm with an average diameter larger than 4 μm. No adhesion between PBS matrix and HDPE domains was observed. The SEM image of PEgMA-added S7E3M is shown in Figure 1(b). The pulled-out HDPE domains were less often detected compared with those in S7E3, and the average

 doi:10.20944/preprints202310.1171.v1

domain size (some with elongated shape) was drastically reduced to ca. 2 μm. The loading of PEgMA had compatibilized PBS with HDPE through the interaction between the ester linkage of PBS and the MA of PEgMA (miscible with HDPE domains) [5]. Figs. 1(c) and 1(d) show the images of S7E3MA3 and S7E3MB3, respectively. A quasi-connected structure of HDPE domains was evident in both composites. However, it was difficult to detect the location of either 15A or 30B in the blend matrix. Figure 1(e) depicts the image of S7E3MT3, in which the HDPE domains likewise became quasi-connected. As revealed in the higher magnification image (Figure 1(f)), CNTs were mainly seen in connected HDPE domains due to their non-polar characteristic. A small amount of CNTs was also discernible in the PBS phase. Figure 1(g) depicts the SEM image of S7E3MG3. The larger-sized GNPs (arrowed) were generally located in the HDPE domains and at the interface of PBS-HDPE phases, with some agglomeration. The above modification in phase-separated morphology of S7E3M after adding individual nanofillers was ascribed to the alteration of the viscosity ratio between PBS and HDPE phases and the selective localization of added fillers (see following rheological/TEM results).

The dispersion of 15A and 30B in the composites was inspected by TEM. Figure 2(a) depicts the image of S7E3MA3. 15A was mainly dispersed in HDPE domains, but some was found at the interface between PBS-HDPE phases. The connected domains of HDPE were observed, consistent with the SEM results. As shown in Figure 2(b), 30B was also mostly located in the connected HDPE domains. The dispersion status (some aggregation) of 30B was inferior to that of 15A, which could be due to the better affinity between 15A and the less polar HDPE/PEgMA compared with that of 30B and HDPE/PEgMA.

Preprints (www.preprints.org) | NOT PEER-REVIEWED | Posted: 18 October 2023 doi:10.20944/preprints202310.1171.v1

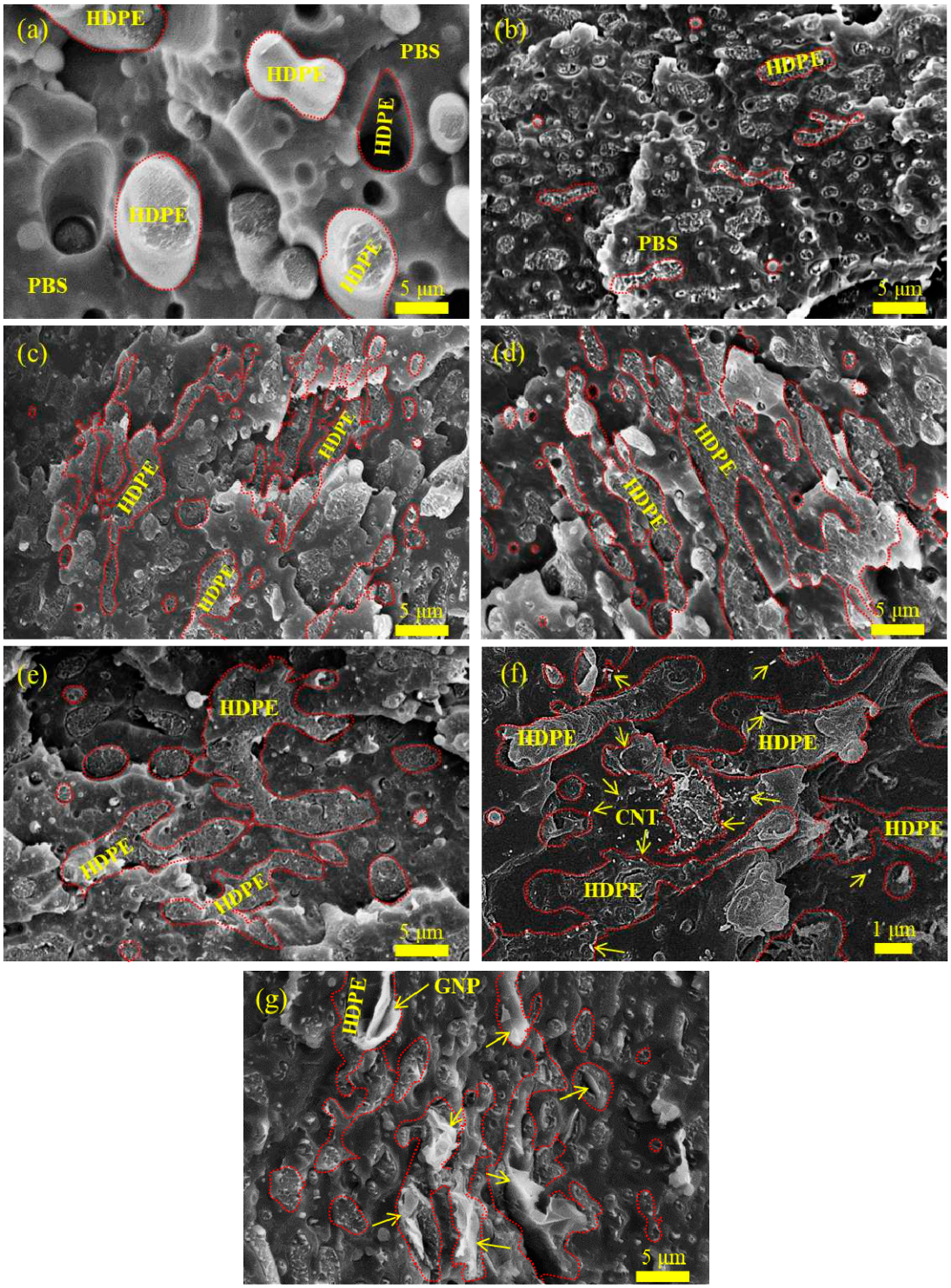

Figure 1. SEM images of representative samples: (a) S7E3, (b) S7E3M, (c) S7E3MA3, (d) S7E3MB3, (e) S7E3MT3, (f) Higher magnification SEM image of S7E3MT3, and (g) S7E3MG3.

Preprints (www.preprints.org) | NOT PEER-REVIEWED | Posted: 18 October 2023 doi:10.20944/preprints202310.1171.v1

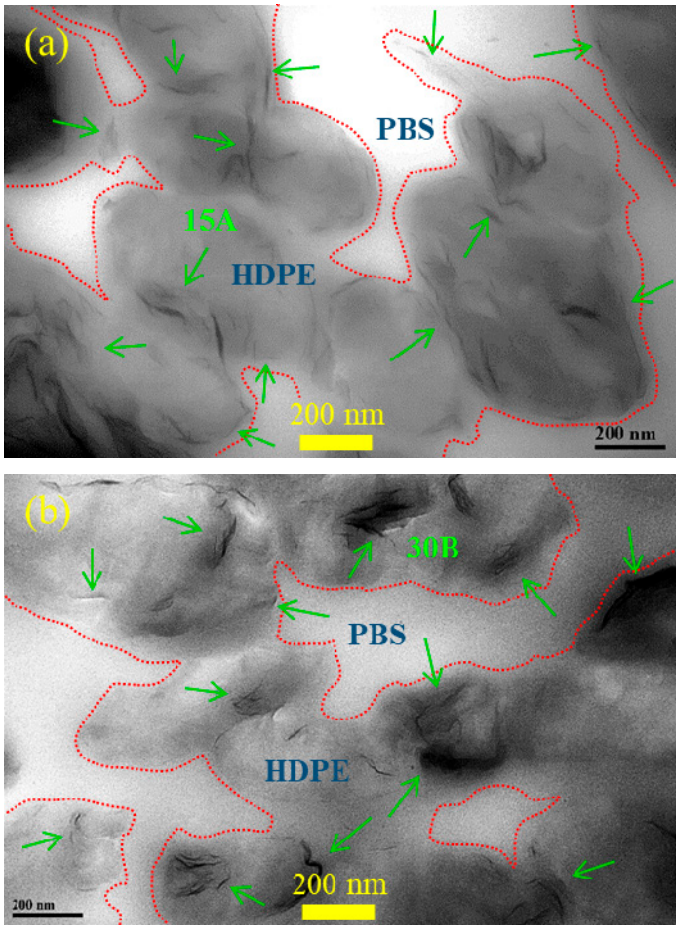

Figure 2. TEM images of selected samples: (a) S7E3MA3 and (b) S7E3MB3.

3.2. Crystallization and melting behavior

Figure 3(a) displays DSC curves of selected samples at 10°C/min cooling from the melt state. The crystallization peak temperatures (T_ps) of PBS and HDPE were 76.1°C and 117.3°C, respectively. In S7E3, the T_p of PBS increased but T_p did not change for HDPE. Hence, the pre-solidified HDPE showed a nucleation effect for PBS crystallization. The existence of PEgMA in S7E3 (cf. S7E3M) resulted in drastically increased T_p of PBS, whereas T_p of HDPE slightly increased. The enhanced affinity (compatibility) of pre-solidified PEgMA/HDPE to PBS and the more dispersed HDPE domains both led to higher nucleation efficiency for PBS crystallization. Regarding the composites, T_p of PBS remained higher than that of neat PBS; T_p of HDPE was marginally changed due to its intrinsically fast crystallization characteristic. However, the individual incorporation of 3 phr 15A and 30B decreased the T_p of PBS compared with that of the parent S7E3M. The retarded crystallization of PBS could be associated with the development of quasi-connected HDPE domains, which caused less HDPE/PEgMA phase-induced nucleation sites for PBS crystallization. S7E3MB3 was seen to display a higher PBS T_p than that of S7E3MA3, which could be ascribed to a higher affinity of 30B (more polar) to PBS than that of 15A (less polar). Some 30B might be located at the PBS phase to facilitate PBS nucleation. The difference in the phase modification of HDPE domains after adding 15A and 30B individually should also be taken into account for the observation. Regarding S7E3MT3 and S7E3MG3, T_p of PBS was higher than that of S7E3MB3, close to that of S7E3M. CNTs and GNPs, partially localized at the interface of PBS-HDPE phases, exhibited a nucleation effect for PBS crystallization and thus compensated for the retarded nucleation caused by the development of quasi-connected HDPE domains.

Figure 3(b) depicts the melting behavior of 10°C/min pre-cooled samples heated at 20°C/min in DSC experiments. A shallow exotherm followed by the main melting peak

 doi:10.20944/preprints202310.1171.v1

(melting-recrystallization-remelting) was observed in neat PBS, in which the main melting at approximately 114°C (T_{mII}) was characterized as peak II. Neat HDPE displayed a simple melting at around 135°C (T_m). For the S7E3 blend, a minor melting peak I (combined with recrystallization) along with the subsequent main melting peak II of PBS was seen. Compared with neat components, T_{mII} of PBS hardly changed and T_m of HDPE slightly decreased in S7E3. Unlike S7E3, S7E3M and the composites showed an evident melting peak I (arrowed, around 107°C) prior to the main melting peak II of PBS, and the peak II shifted to a higher temperature compared with those of S7E3 and neat PBS. T_m of HDPE was also slightly higher in the composites than in S7E3. The melting behavior change after forming S7E3M and the composites indicated that the added PEgMA and fillers had induced more stable PBS and HDPE crystal growth. The nucleation effect of PEgMA and added fillers played a role in this observation. Figure 4 shows the XRD results of samples cooled at 10°C/min from the melt state. Neat PBS showed two diffractions (monoclinic structure) at $2\theta = 19.0°$ (020) and 22.1° (110) [5,17], whereas HDPE revealed two diffractions (orthorhombic structure) at $2\theta = 20.8°$ (110) and 23.1° (200) [5]. Diffractions of both PBS and HDPE crystals were seen in the blends and composites. Additionally, S7E3MG3 showed a strong diffraction peak at $2\theta = 25.8°$, attributed to the layered structure of GNPs. The XRD results confirmed that the formations of blends and composites did not alter the crystal structures of PBS and HDPE.

Preprints (www.preprints.org) | NOT PEER-REVIEWED | Posted: 18 October 2023 doi:10.20944/preprints202310.1171.v1

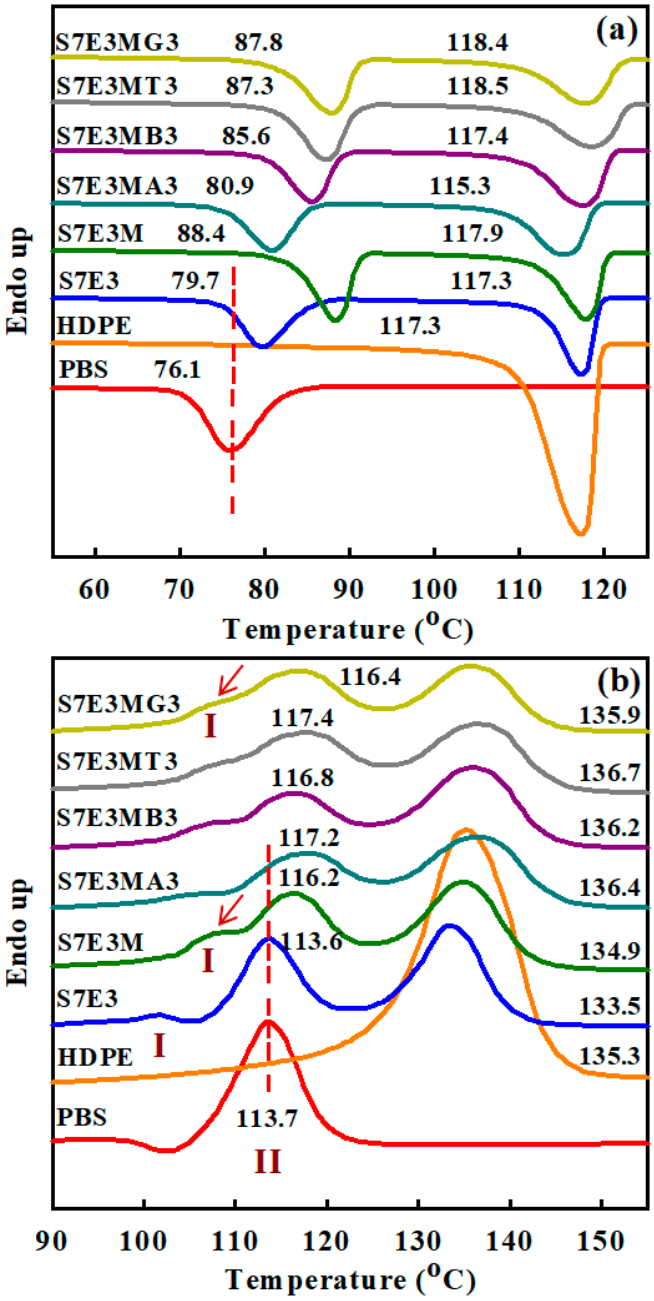

Figure 3. (a) DSC curves of the samples at 10°C/min cooling; (b) DSC heating curves of the samples pre-cooled at 10°C/min.

Preprints (www.preprints.org) | NOT PEER-REVIEWED | Posted: 18 October 2023 doi:10.20944/preprints202310.1171.v1

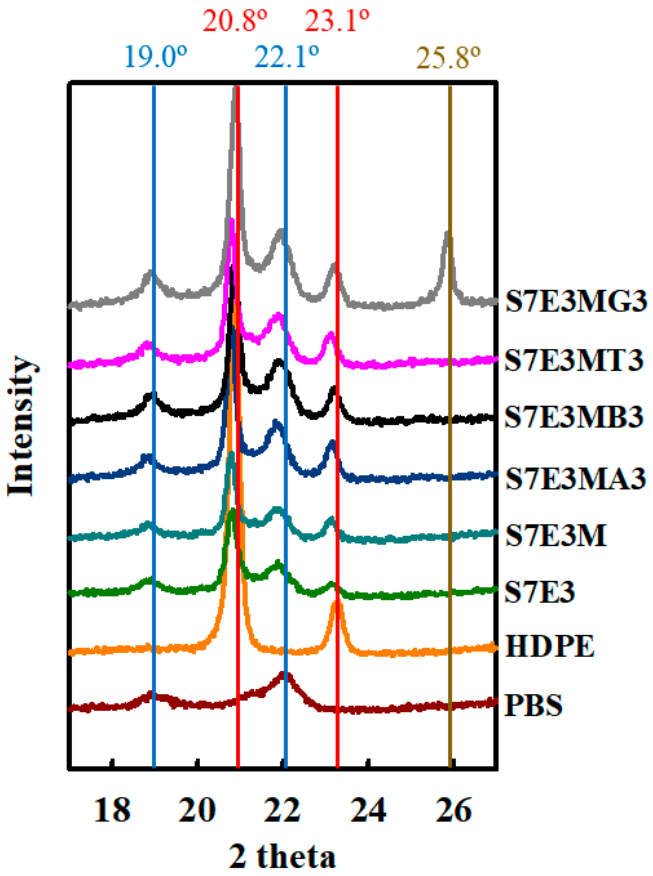

Figure 4. XRD patterns of 10°C/min-cooled samples.

3.3. Thermal stability

TGA curves of selected samples are shown in Figure 5. HDPE showed higher thermal stability than PBS, with a temperature at 10 wt.% loss (T_{d10}) of around 435°C for HDPE and 369°C for PBS. After forming the blends and composites, two-step degradations were seen, corresponding to the individual degradation of PBS and HDPE. Comparing the T_{d10} of individual samples (Table 2), it is concluded that the development of quasi-connected HDPE domains in the composites hardly retarded the initial degradation of PBS matrix (similar T_{d10}), except that the added GNP showed some enhancing effect. A dotted vertical line was drawn in the figure at 425°C, to indicate the start point for serious degradation of neat HDPE. It is observed that the start point for HDPE serious degradation evidently shifted to higher temperatures in the composites, particularly for CNT- and GNP-included composites. This result was attributed to the fillers with outstanding thermal stability being mostly located in the HDPE domains. Moreover, CNTs and GNPs could supply additional free radical scavenging functionality [6]. T_{d90} (90 wt.% loss temperature) of the composites followed the sequence of added fillers: GNP>CNT>30B≒15A. The layered nature of GNPs retarded the evaporation of degraded molecules to a greater degree, thus showing superior enhancement of thermal stability of the composites compared with CNTs.

Table 2. Thermal, mechanical, and electrical property data of fabricated samples.

Samples	Properties				
	T_{d10} (°C)	T_{d90} (°C)	YM (MPa) (σ)	FM (MPa) (σ)	Log (volume resistivity) (Ω-cm)
PBS	369	419	515 ± 34	245 ± 7	>14
HDPE	435	488	836 ± 25	269 ± 25	>14
S7E3	370	484	551 ± 54	251 ± 12	>14

Preprints (www.preprints.org) | NOT PEER-REVIEWED | Posted: 18 October 2023 doi:10.20944/preprints202310.1171.v1

S7E3M	368	475	676 ± 54	284 ± 10	>14
S7E3MA3	368	489	756 ± 29	331 ± 12	>14
S7E3MB3	367	490	707 ± 19	303 ± 9	>14
S7E3MT3	368	495	719 ± 47	311 ± 25	7.5 ± 0.1
S7E3MG3	373	499	803 ± 29	373 ± 20	>14

σ: Standard deviation.

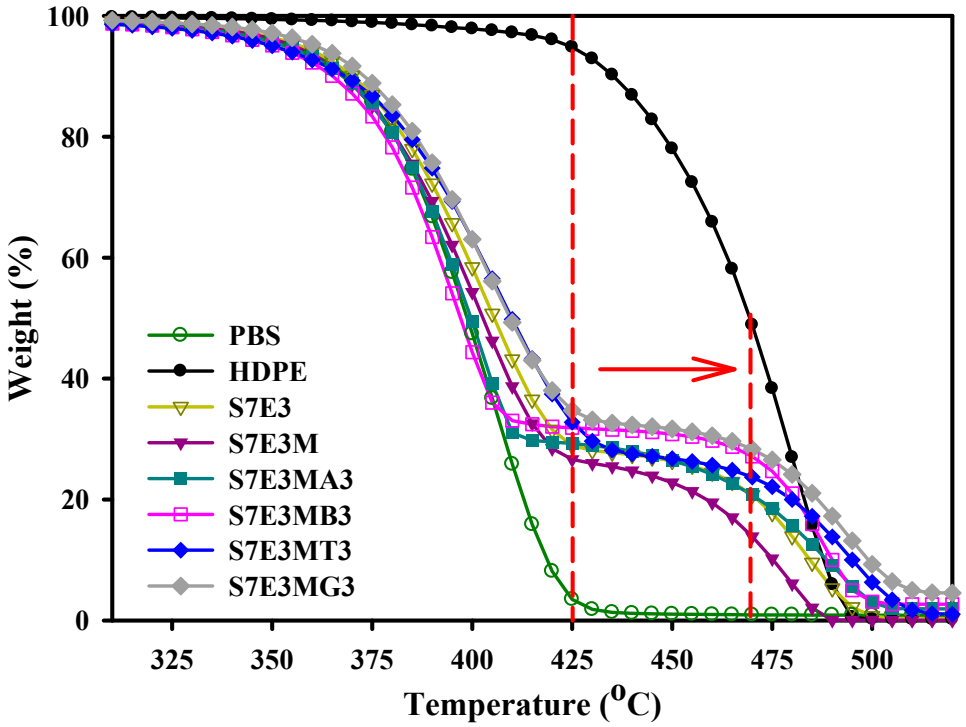

Figure 5. TGA curves of the samples scanned under N_2 environment.

3.4. Anti-dripping performance

The effects of adding PEgMA and nanofillers on the anti-dripping performance for the S7E3 blend are shown in Figure 6 as digital photos of selected specimens at various time intervals. S7E3 (Figure 6(a)) kept burning after being removed from the flame source and then showed melt dripping after 13 s, leading to viscous flow-like behavior. S7E3 showed severe melt dripping (more than 40 droplets) up to 40 s of burning, indicating poor melt dripping performance. The compatibilized S7E3M displayed melt dripping at a delayed time of 31 s [Figure 6(b)], and the flame area/size was smaller compared with S7E3 at the identical time. The improved anti-dripping behavior of S7E3M could result from it having better dispersion of HDPE domains. S7E3M showed only 4 melt droplets for 40 s of burning. Figs. 6(c) and 6(d) display the burning performance of S7E3MA3 and S7E3MB3, respectively. After continuous burning for 40 s, no melt droplets were observed for both S7E3MA3 and S7E3MB3 composites, indicating that the presence of 15A and 30B improved the anti-dripping properties of S7E3M blend. Similarly, S7E3MT3 [Figure 6(e)] showed no melt droplets after 40 s of burning. The flame size of S7E3MT3 was smaller than that of S7E3M. Regarding S7E3MG3 [Figure 6(f)], it displayed inferior anti-dripping performance compared with the other composites. Melt droplets were noticed after 48 s of burning, which could be attributed to the less good dispersion of GNPs in S7E3M matrix (mainly in HDPE domains). The improved anti-dripping performance observed for the composites resulted from the formation of quasi connected filler-included HDPE domains having higher melt strength than the PBS matrix. The burning test process (see supplementary video) showed that S7E3MT3 did not reveal any dripping after 80 s, whereas S7E3MA3, S7E3MB3 and S7E3MG3 showed dripping after 75 s, 57 s and 48 s, respectively. Hence, it was demonstrated that S7E3MT3 possessed improved anti-dripping

Preprints (www.preprints.org) | NOT PEER-REVIEWED | Posted: 18 October 2023 doi:10.20944/preprints202310.1171.v1

performance compared with S7E3MA3, S7E3MB3 and S7E3MG3. The improvement of anti-dripping performance by adding fillers for S7E3M followed the sequence of: CNT>15A>30B>GNP.

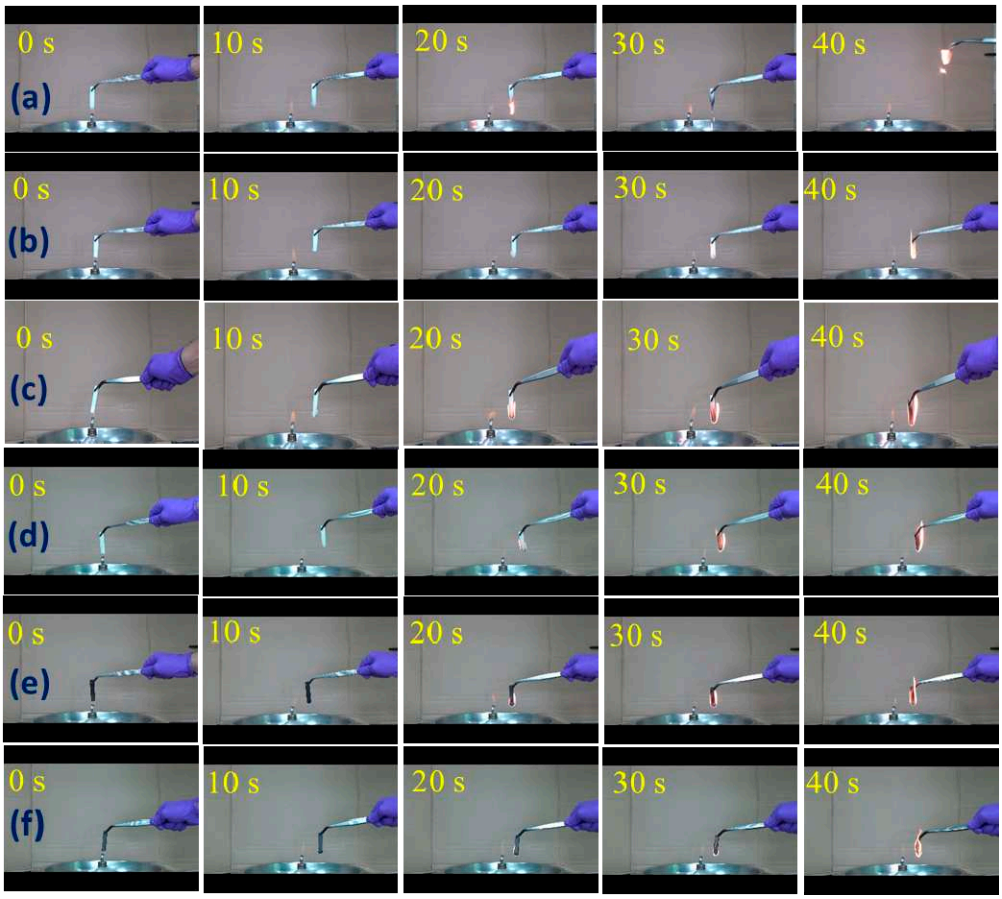

Figure 6. Digital photos of combustion process at different times of: (a) S7E3, (b) S7E3M, (c) S7E3MA3, (d) S7E3MB3, (e) S7E3MT3, and (f) S7E3MG3.

3.5. Mechanical properties

Figure 7(a) depicts typical stress-strain curves of selected samples. Young's modulus (YM) and flexural modulus (FM) of the samples are compared in Figure 7(b) and 7(c), respectively. The data are listed in Table 2. Neat HDPE had a higher YM than neat PBS. The YM of S7E3 was in between the two neat components, and was lower than the value (611) calculated by the law of additivity (attributed to the blend's evidently incompatible characteristic). After incorporating PEgMA, YM increased to a value higher than 611, demonstrating the enhancement in PBS-HDPE interaction. After loading with different fillers (15A/30B/CNT/GNP), YM further increased. S7E3MA3 showed a higher YM than S7E3MB3, possibly due to the better dispersion of 15A compared with 30B. Of the fillers added, GNPs showed the best efficiency (up to 19%) in enhancing the YM of S7E3M matrix. The intrinsic high modulus and the sheet-like structure of GNPs played the dominant role for achieving the best YM improvement. Similar to the formulation-dependent trend of YM, neat PBS had a FM value lower than that of neat HDPE. FM of S7E3 was in between those of the parent components. After adding PEgMA, FM increased (even higher than neat HDPE) because of the compatibilizing effect of PEgMA. Loading 3-phr of 15A, 30B, CNTs and GNPs into S7E3M matrix increased the FM by 16%, 7%, 10% and 31%, respectively. Efficiency in enhancement of YM and FM followed the sequence of added filler: GNP>15A>CNT>30B. The reasons behind this significant improvement of FM after adding GNPs are identical to those for YM improvement.

Preprints (www.preprints.org) | NOT PEER-REVIEWED | Posted: 18 October 2023 doi:10.20944/preprints202310.1171.v1

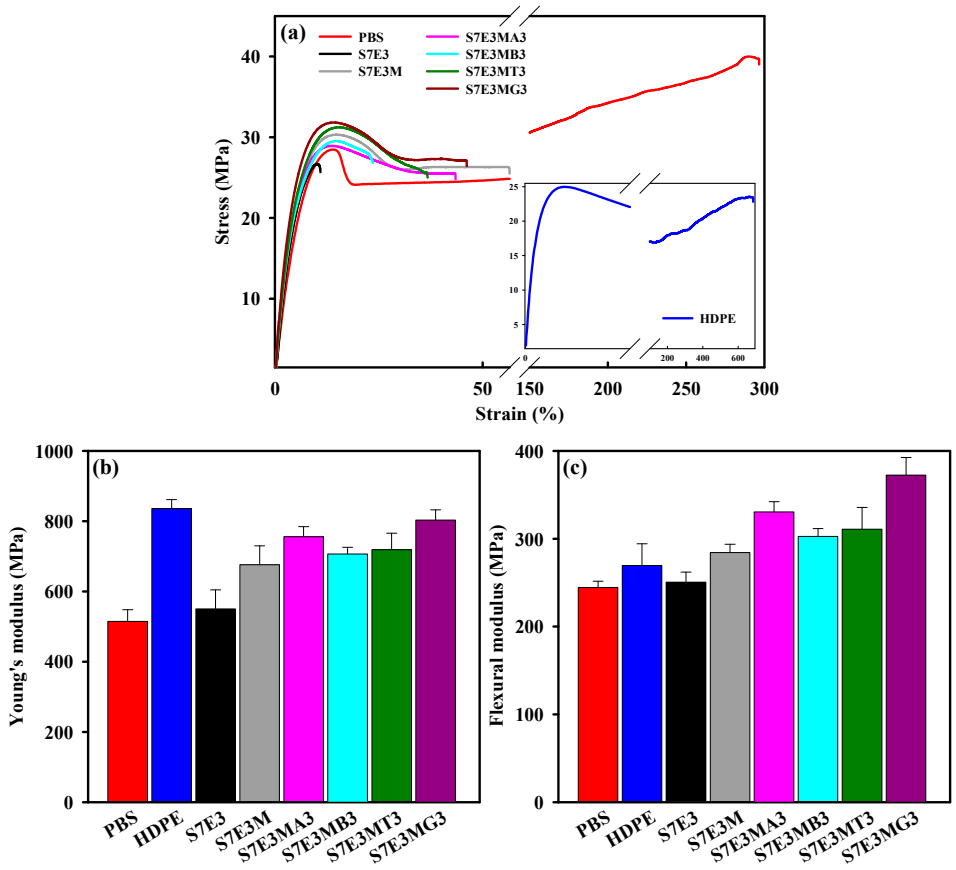

Figure 7. (a) Typical S-S curves, (b) Young's modulus and (c) flexural modulus of the samples.

3.6. Melt rheology

Rheological properties play a vital role in polymer processing and can reveal the internal structure modification after forming blends/composites. Figure 8(a) depicts the complex viscosity (η*) vs. sweep frequency (ω) of the samples. Neat PBS displayed the lowest viscosity and liquid-like (Newtonian fluid) behavior at the test temperature of 170°C. Neat HDPE had higher η* values than PBS at all frequencies; S7E3 had η* values that lay between those of PBS and HDPE. With the incorporation of PEgMA, S7E3M showed higher η* values than those of S7E3 at ω < 3 rad/s, and revealed shear thinning behavior at all frequencies. The behavior of S7E3M could be ascribed to the more dispersed/reduced domain size of HDPE and the improvement of interaction between PBS-HDPE phases. The η* values of S7E3M increased after forming the composites. The added inorganic fillers reduced the fluidity of the polymer matrix under shear tests. Among the composites, S7E3MA3 displayed the highest η* at all frequencies due to the fine dispersion of 15A along with the good interaction between 15A and polymer matrix (mainly HDPE/PEgMA domains). The impact of incorporating individual fillers on η* of S7E3M matrix followed the sequence 15A>CNT>30B>GNP. The inferior dispersibility of GNPs in the composite led to its least effect on η* modification. Moreover, η* showed non-Newtonian fluid (shear thinning) behavior at the frequencies tested for all composites. The shear thinning behavior at low frequencies confirmed the formation of a pseudo-network (solid-like) structure of quasi-connected HDPE domains combined with fine dispersion of nanofillers. The storage modulus (G′) is plotted against ω in Figure 8(b). G′ increased with increasing ω for the samples tested, and the values were higher for the composites compared with the S7E3M parent matrix. A similar formulation-dependent trend to that of η* was observed in the G′ test results. G′ of S7E3 was in between that of neat PBS and HDPE. S7E3MA3 displayed the highest G′ of the composites at all frequencies, by about 1.5 orders of magnitude (at ω <1 rad/s) higher than that of S7E3M. The almost flattened slopes in the plots of S7E3M and composites at low frequencies, agreeing with η* results, signified the development of a

Preprints (www.preprints.org) | NOT PEER-REVIEWED | Posted: 18 October 2023 doi:10.20944/preprints202310.1171.v1

pseudo-network structure (solid-like behavior) within the polymer matrix. Compared with the neat components and blends, increased elastic nature of the composites was confirmed.

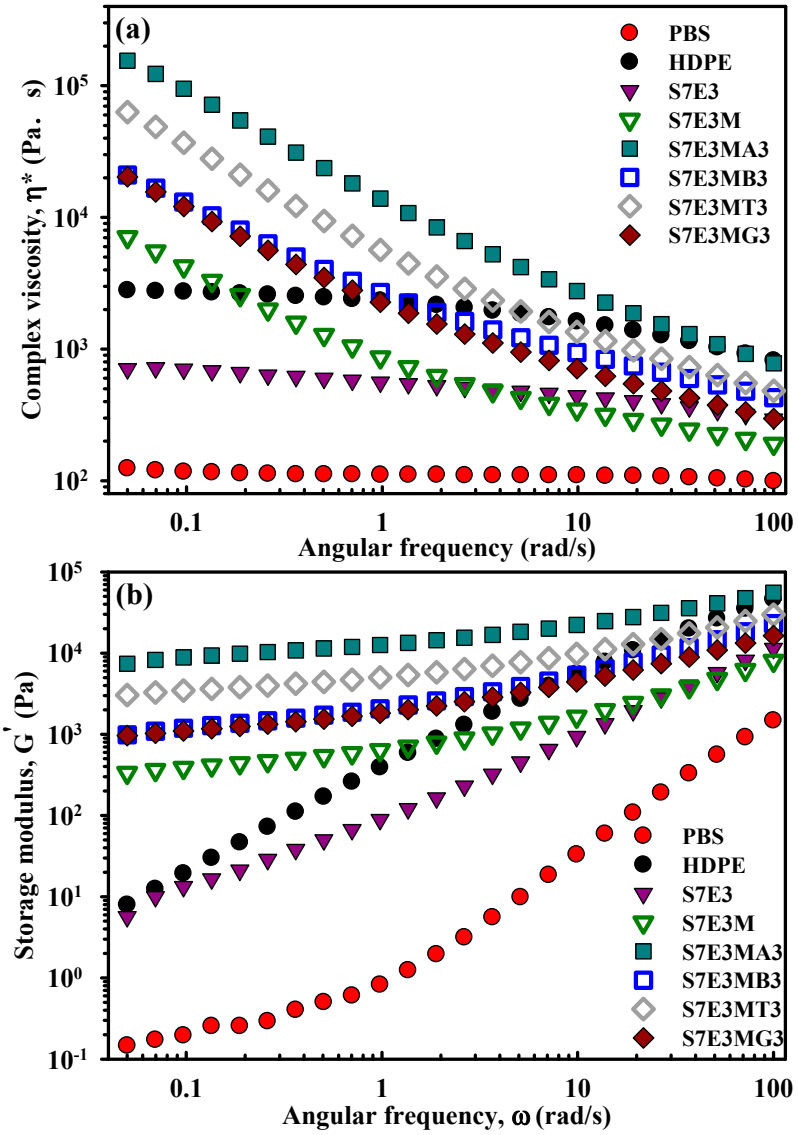

Figure 8. Rheological properties of the samples: (a) η* vs. ω and (b) G′ vs. ω.

3.7. Electrical resistivity

The measured electrical resistivity (ER) values of the samples are included in Table 2. As anticipated, neat components and the blends had ER values of above 1014 Ω-cm. After adding 15A or 30B into S7E3M (i.e., S7E3MA3 and S7E3MB3), ER hardly changed, remaining electrically insulating. Notably, ER value decreased to around 108 Ω-cm for S7E3MT3, more than 6 orders lower compared with parent S7E3M. The fine dispersion of CNTs, mainly in the quasi-connected HDPE domains, was accountable for the evident ER drop, suggesting that double percolation morphology was achieved in S7E3MT3. Nevertheless, with 3 phr GNP loading in S7E3M (S7E3MG3), ER barely decreased due to the inferior dispersibility of multi-layered GNPs in quasi-connected HDPE domains.

4. Conclusions

Immiscible PBS/HDPE blends and blend-based nanocomposites compatibilized with PEgMA were successfully fabricated by melt extrusion. In the composites, the added nanofillers (15A, 30B, CNTs, and GNPs) were mainly localized in HDPE domains, but some were also situated at the

PBS-HDPE interfaces, leading to quasi-connected HDPE domains. With incorporation of PEgMA, crystallization of PBS in the blend was evidently accelerated during the cooling process. The added fillers did not facilitate, and even retarded, the crystallization of PBS, attributed to the combined effects of filler localization mainly in HDPE domains and the formation of quasi-connected HDPE domains (less nucleation sites for PBS crystallization). The crystallization of HDPE barely changed in the blends/composites due to its intrinsic fast crystallization characteristic. PEgMA and fillers induced more stable PBS crystals to grow in the compatibilized blend and composites. Composites showed higher thermal stability compared with the parent blend, particularly in enhancement for the HDPE portion. An improvement in anti-dripping performance in burning tests was found for the composites compared with the blends, with improvement efficiency following the sequence of added fillers: CNT>15A>30B>GNP. Rigidity of the blend improved after development of composites; the effectiveness in increasing rigidity followed the sequence of added fillers: GNP>15A>CNT>30B. Rheological properties suggested the formation of a pseudo-network structure in the composites. Electrical resistivity of the blend matrix decreased by more than 6 orders of magnitude to around 108 Ω-cm at 3 phr CNT loading.

Author Contributions: Conceptualization, K.B. and F.-C.C.; Investigation, K.B. and C.-H.T.; Methodology, K.B. and C.-H.T.; Software, K.B. and C.-H.T.; Data curation, K.B. and C.-H.T.; Formal analysis, K.B.; Visualization, K.B. and C.-H.T.; Validation, K.B. and C.-H.T.; Writing- Original draft preparation. K.B.; Resources, F.-C.C. and Y.-H.C.; Writing- review & editing, K.B. and F.-C.C.; Supervision, F.-C.C.; Project administration, F.-C.C.; Funding acquisition, F.-C.C. and Y.-H.C. All authors have read and agreed to the published version of the manuscript.

Funding: We gratefully acknowledge the financial support to carry out this research work from (1) Chang Gung Memorial Hospital (Taoyuan, Taiwan): CMRPD2M0271, (2) National Science and Technology Council (NSTC, Taiwan): NSTC 109-2221-E-182-056-MY3, NSTC 109-2221-E-182-057-MY3 and NSTC 112-2811-E-182-005-MY3. The authors also thank the Microscopy Center at Chang Gung University for technical assistance.

Institutional Review Board Statement: Not applicable.

Informed Consent Statement: Not applicable

Data Availability Statement: Data sharing not applicable.

Conflicts of Interest: The authors declare no conflict of interest.

References

1. Ray, S.S.; Bousmina, M. Biodegradable polymers and their layered silicate nanocomposites: In greening the 21st century materials world. *Prog. Mater. Sci.* **2005**, 50, 962-1079.
2. Lin, H.M.; Behera, K.; Yadav, M.; Chiu, F.C. Polyamide 6/poly(vinylidene fluoride) blend-based nanocomposites with enhanced rigidity: Selective localization of carbon nanotube and organoclay. *Polymers* **2020**, 12, 184-199.
3. Behera, K.; Chen, J.F.; Yang, J.M.; Chang, Y.H.; Chiu, F.C. Evident improvement in burning anti-dripping performance, ductility and electrical conductivity of PLA/PVDF/PMMA ternary blend-based nanocomposites with additions of carbon nanotubes and organoclay. *Compos. B. Eng.* **2023**, 248, 110371-110382.
4. Chiu, F.C.; Behera, K.; Cai, H.J.; Chang, Y.H. Polycarbonate/poly(vinylidene fluoride)-blend-based nanocomposites—Effect of adding different carbon nanofillers/organoclay. *Polymers* **2021**, 13, 26261-26276.
5. Darshan T.G.; Veluri, S.; Behera, K.; Chang, Y.H.; Chiu, F.C. Poly(butylene succinate)/high density polyethylene blend-based nanocomposites with enhanced physical properties – Selectively localized carbon nanotube in pseudo-double percolated structure. *Polym. Degrad. Stab.* **2019**, 163, 185-194.
6. Behera, K.; Chang, Y.H.; Chiu, F.C. Manufacturing poly(butylene adipate-co-terephthalate)/high density polyethylene blend-based nanocomposites with enhanced burning anti-dripping and physical properties — Effects of carbon nanofillers addition. *Compos. B Eng.* **2021**, 217, 108878-108889.
7. Ray, S.S.; Maiti, P.; Okamoto, M.; Yamada, K.; Ueda, K. New polylactide/layered silicate nanocomposites. 1. Preparation, characterization, and properties. *Macromolecules* **2002**, 35, 3104-3110.
8. Sivanjineyulu V.; Chang, Y.H.; Chiu, F.C. Characterization of carbon nanotube- and organoclay-filled polypropylene/poly(butylene succinate) blend-based nanocomposites with enhanced rigidity and electrical conductivity. *J. Polym. Res.* **2017**, 24, 130-142.

9. Jacquel, N.; Freyermouth, F.; Fenouillot, F.A.; Rousseau, J.P.; Pascault, P.; Loup, R.S. Synthesis and properties of poly(butylene succinate): Efficiency of different transesterification catalysts. *J. Polym. Sci. Part A: Polym. Chem.* **2011**, 49, 5301-5312.
10. Gigli, M.; Fabbri, M.; Lotti, N.; Gamberini, R.; Rimini, B.; Munari, A. Poly(butylene succinate)-based polyesters for biomedical applications: A review. *Eur. Polym. J.* **2016**, 75, 431-460.
11. Bleija, M.; Platnieks, O.; Macutkevič, J.; Banys, J.; Starkova, O.; Grase, L.; Gaidukovs, S. Poly(butylene succinate) hybrid multi-walled carbon nanotube/iron oxide nanocomposites: Electromagnetic shielding and thermal properties. *Polymers* **2023**, 15, 515-534.
12. Amornsakchai, T.; Duangsuwan, S.; Mougin, K.; Goh, K.L. Comparative study of flax and pineapple leaf fiber reinforced poly(butylene succinate): Effect of fiber content on mechanical properties. *Polymers* **2023**, 15, 3691-3706.
13. Barletta, M.; Aversa, C.; Ayyoob, M.; Gisario, A.; Hamad, K.; Mehrpouya, M.; Vahabi, H. Poly(butylene succinate) (PBS): Materials, processing, and industrial applications. *Prog. Polym. Sci.* **2022**, 132, 101579-101641.
14. Aontee, A.; Sutapun, W. Effect of blend ratio on phase morphology and mechanical properties of high density polyethylene and poly(butylene succinate) blend. *Adv. Mater. Res.* **2013**, 747, 555-559.
15. Luo, X.; Li, J.; Feng, J.; Yang, T.; Lin, X. Mechanical and thermal performance of distillers grains filled poly(butylene succinate) composites. *Mater. Des.* **2014**, 57, 195-200.
16. Chen, J.B.; Xu, J.Z.; Xu, H.; Li, Z.M.; Zhong, G.J.; Lei, J. The crystallization behavior of biodegradable poly(butylene succinate) in the presence of organically modified clay with a wide range of loadings. *Chinese J. Polym. Sci.* **2015**, 33, 576-586.
17. Teng, J.; Niu, B.; Zhang, L.Q.; Ji, X.; Xu, L.; Yan, Z.; Tang, J.H.; Zhong, G.J.; Li, Z.M. Confined crystallization of poly(butylene succinate) intercalated into organoclays: role of surfactant polarity. *RSC Adv.* **2016**, 6, 68072-68080.
18. Yuan, L.; Wu, D.; Zhang, M.; Zhou, W.; Lin, D. Rheological percolation behavior and isothermal crystallization of poly(butyene succinte)/carbon nanotube composites. *Ind. Eng. Chem. Res.* **2011**, 50, 14186-14192.
19. Platnieks, O.; Gaidukovs, S.; Neibolts, N.; Barkane, A.; Gaidukova, G.; Thakur, V.K. Poly(butylene succinate) and graphene nanoplatelete based sustainable functional nanocomposite materials: structure-properties relationship. *Mater. Today Chem.* **2020**, 18, 100351-100359.
20. Yu, S.; Lee, J.; Kim, J.; Chang, H.; Kang, C.; Sim, J. Analysis of mechanical properties and structural analysis according to the multi-layered structure of polyethylene-based self-reinforced composites. *Polymers* **2023**, 15, 4055-4070.
21. Shah, A.U.R.; Jalil, A.; Sadiq, A.; Alzaid, M.; Naseem, M.S.; Alanazi, R.; Alanazi, S.; Alanzy, A.O.; Alsohaimi, I.H.; Malik, R.A. Effect of rice husk and wood flour on the structural, mechanical, and fire-retardant characteristics of recycled high-density polyethylene. *Polymers* **2023**, 15, 4031-4046.
22. Zhang, X.M.; Elkoun, S.; Ajji, A.; Huneault, M.A. Oriented structure and anisotropy properties of polymer blown films: HDPE, LLDPE and LDPE. *Polymer* **2004**, 45, 217-229.
23. Brandalise, R.N.; Zeni, M.; Martins, J.D.N.; Forte, M.M.C. Morphology, mechanical and dynamic mechanical properties of recycled high density polyethylene and poly(vinyl alcohol) blends. *Polym. Bull.* **2009**, 62, 33-43.
24. Minkova, L.; Filippi, S. Characterization of HDPE-g-MA/clay nanocomposites prepared by different preparation procedures: Effect of the filler dimension on crystallization, microhardness and flammability. *Polym. Test.* **2011**, 30, 1-7.
25. Aontee, A.; Sutapun, W. A study of compatibilization effect on physical properties of poly(butylene succinate) and high density polyethylene blend. *Adv. Mater. Res.* **2013**, 699, 51-56.
26. Kodjie, S.L.; Li, L.; Li, B.; Cai, W.W.; Li, C.Y.; Keating, M. Morphology and crystallization behavior of HDPE/CNT nanocomposite. *J. Macromol. Sci. B Phys.* **2006**, 45, 231-245.
27. Tarani, E.; Wurm, A.; Schick, C.; Bikiaris, D.N.; Chrissafis, K.; Vourlias, G. Effect of graphene nanoplatelets diameter on non-isothermal crystallization kinetics and melting behavior of high density polyethylene nanocomposites. *Thermochim. Acta* **2016**, 643, 94-103.
28. Morawiec, J.; Pawlak, A.; Slouf, M.; Galeski, A.; Piorkowska, E.; Krasnikowa, N. Preparation and properties of compatibilized LDPE/organo-modified montmorillonite nanocomposites. *Eur. Polym. J.* **2005**, 41, 1115-1122.
29. Gcwabaza, T.; Ray, S.S.; Focke, W.W.; Maity, A. Morphology and properties of nanostructured materials based on polypropylene/poly(butylene succinate) blend and organoclay. *Eur. Polym. J.* **2009**, 45, 353-367.
30. Bhatia, A.; Gupta, R.; Bhattacharya, S.; Choi, H. Effect of clay on thermal, mechanical and gas barrier properties of biodegradable poly(lactic acid)/poly(butylene succinate) (PLA/PBS) nanocomposites. *Int. Polym. Process.* **2010**, 25, 5-14.

31. Ojijo, V.; Sinha Ray, S.; Sadiku, R. Effect of nanoclay loading on the thermal and mechanical properties of biodegradable polylactide/poly[(butylene succinate)-co-adipate] blend composites. *ACS Appl. Mater. Interfaces* **2012**, 4, 2395-2405.
32. Wu, W.; Wu, C.; Peng, H.; Sun, Q.; Zhou, L.; Zhuang, J.; Cao, X.; Roy, V.A.L.; Li, R.K.Y. Effect of nitrogen-doped graphene on morphology and properties of immiscible poly(butylene succinate)/polylactide blends. *Compos. B Eng.* **2017**, 113, 300-307.
33. Chiu, F.C.; Yen, H.Z.; Chen, C.C. Phase morphology and physical properties of PP/HDPE/organoclay (nano) composites with and without a maleated EPDM as a compatibilizer. *Polym. Test.* **2010**, 29, 706-716.